IOP Publishing | Institute of Physics and Engineering in Medicine Physics in Medicine & Biology

Phys. Med. Biol. **62** (2017) 146–164 doi:10.1088/1361-6560/aa4f6a

Collision-kerma conversion between dose-to-tissue and dose-to-water by photon energy-fluence corrections in low-energy brachytherapy

Vicent Giménez-Alventosa[1], Paula C G Antunes[1,2], Javier Vijande[1,3], Facundo Ballester[1], José Pérez-Calatayud[4,5] and Pedro Andreo[6]

[1] Department of Atomic, Molecular, and Nuclear Physics, University of Valencia, E46100 Burjassot, Spain
[2] Instituto de Pesquisas Energéticas e Nucleares—IPEN-CNEN/SP, São Paulo, Brazil
[3] Instituto de Física Corpuscular (UV-CSIC), 46100 Burjassot, Spain
[4] Radiation Oncology Department, La Fe University and Polytechnic Hospital, Valencia, Spain
[5] Department of Radiotherapy, Clínica Benidorm, 03501 Benidorm, Spain
[6] Department of Medical Physics, Karolinska University Hospital, SE-171 76 Stockholm, Sweden

E-mail: vijande@uv.es

Received 22 September 2016, revised 4 November 2016
Accepted for publication 23 November 2016
Published 16 December 2016

Abstract

The AAPM TG-43 brachytherapy dosimetry formalism, introduced in 1995, has become a standard for brachytherapy dosimetry worldwide; it implicitly assumes that charged-particle equilibrium (CPE) exists for the determination of absorbed dose to water at different locations, except in the vicinity of the source capsule. Subsequent dosimetry developments, based on Monte Carlo calculations or analytical solutions of transport equations, do not rely on the CPE assumption and determine directly the dose to different tissues. At the time of relating dose to tissue and dose to water, or vice versa, it is usually assumed that the photon fluence in water and in tissues are practically identical, so that the absorbed dose in the two media can be related by their ratio of mass energy-absorption coefficients. In this work, an efficient way to correlate absorbed dose to water and absorbed dose to tissue in brachytherapy calculations at clinically relevant distances for low-energy photon emitting seeds is proposed. A correction is introduced that is based on the ratio of the water-to-tissue photon energy-fluences. State-of-the art Monte Carlo calculations are used to score photon fluence differential in energy in water

and in various human tissues (muscle, adipose and bone), which in all cases include a realistic modelling of low-energy brachytherapy sources in order to benchmark the formalism proposed. The energy-fluence based corrections given in this work are able to correlate absorbed dose to tissue and absorbed dose to water with an accuracy better than 0.5% in the most critical cases (e.g. bone tissue).

Keywords: Monte Carlo, dosimetry, low-energy seed, collision-kerma, mass energy-absorption coefficients, energy-fluence correction factor

(Some figures may appear in colour only in the online journal)

1. Introduction

The AAPM TG-43 brachytherapy dosimetry formalism, introduced in 1995 and modified subsequently in various publications (Nath *et al* 1995, Rivard 2004, 2007, Rivard *et al* 2010), has become a standard for brachytherapy dosimetry worldwide. This formalism implicitly assumes that a seed is embedded in an infinite water medium and, consequently, charged-particle equilibrium (CPE) exists (except at short distances from the source capsule). At low photon energies the radiation yield of the photon-generated electrons is practically negligible; absorbed dose can, therefore, be approximated by collision kerma. Monte Carlo and experimentally derived TG-43 consensus datasets for both high- and low-energy sources have been extensively derived in the literature based on these approximations (Dolan *et al* 2006, Rivard *et al* 2006, Sowards 2007, Perez-Calatayud *et al* 2012).

Currently, most of the clinical experience is mainly based on TG-43, i.e. absorbed dose-to-water in water. However, it is well known that the TG-43 assumptions may not be accurate in some clinical situations (Carlsson-Tedgren and Alm-Carlsson *et al* 2013). This is particularly true for the combination of low-energy photons (<100 keV) and some tissues as bone, for which the ratio of mass energy-absorption coefficients $(\mu_{en}/\rho)^{w}_{tis}$ are significantly different from unity. The high-Z elements found in bone structures make the photoelectric effect to be the predominant interaction, leading to a higher absorption of low-energy photons and therefore hardening the photon spectrum as it goes deeper on the body (Fonseca *et al* 2015). Body-air interfaces, like those observed in breast or lung lesions, are another clinical situations where TG-43 assumptions are not valid (Afsharpour *et al* 2011, Landry *et al* 2011, Sutherland *et al* 2012).

In this context, state-of-the-art model-based dose calculations algorithms (MBDCAs) (Beaulieu *et al* 2012) such as Monte Carlo (MC) and analytical models like ACE (advanced calculation engine—nucletron—an Elekta Company, Veenendaal, The Netherlands) (Carlsson-Tedgren and Ahnesjö 2008, Ahnesjö 2013, Van Veelen *et al* 2014) and ACUROS^{TM} (Transpire Inc., Gig Harbor, WA) (Petrokokkinos *et al* 2011, Lloyd and Ansbacher 2013), both for HDR applications with ^{192}Ir, have become available in brachytherapy. They are considered by AAPM TG-186 as potential replacements of the TG-43 formalism. MBDCAs are capable of handling tissue compositions/densities and other treatments complexities leading to the determination of dose-to-tissue. Tissue compositions/densities can be obtained from dual-CT procedures, or from single-CT using a lookup table, although constraints on the current procedures for tissue segmentation have been pointed out by Andreo (2015) for tissues having identical or very similar density.

The relation between dose-to-tissue and dose-to-water, or vice versa, has been the subject of some recent publications in order to associate all previous clinical experience based on dose-to-water with the new methodologies based on dose-to-tissue. See Beaulieu *et al* (2012), Andreo (2015), Ballester *et al* (2015), Kumar *et al* (2016), and references therein.

Usually, absorbed dose calculations are performed using cavity theory in which the cavity dimensions are compared to the ranges of secondary electrons (Attix 1986). When the cavity is larger than the range of secondary electrons, the absorbed dose to non-water tissue is estimated using ratios of mass energy-absorption coefficients between water and tissue (Landry *et al* 2011, Carlsson-Tedgren and Alm-Carlsson *et al* 2013), on the assumption that the photon energy-fluence at the point of interest is practically the same for water and for the different human tissues.

The purpose of this work is to study the influence of photon energy-fluence in different media and to evaluate a proposal for energy-fluence correction factors for the conversion between dose-to-tissue and dose-to-water. For this goal, Monte Carlo simulations for a subset of human tissues of interest in brachytherapy for three low-energy brachytherapy seeds (^{103}Pd, ^{125}I, and ^{131}Cs) have been performed.

2. Materials and methods

This section describes the methodology employed to convert absorbed dose to a tissue (D_{tis}) into absorbed dose to water (D_{w}) using the large-cavity theory and how Monte Carlo calculations have been carried out. The method is also applicable to the reverse conversion, i.e. from D_{w} to D_{tis}, after the proper reversal of subscripts.

2.1. Relation between D_{w} and D_{tis}

At this point it should be emphasized that the conversion between D_{tis} and D_{w} is required mainly due to:

(a) most treatment planning systems (TPS) calculate D_{w}, hence currently available clinical experience is mostly based on D_{w};
(b) advanced developments in absorbed dose calculation methods (e.g. MBDCAs) are able to determine accurately D_{tis} assuming that a valid characterization of tissues from dual-CT procedures or from a lookup density-tissue table has been made;
(c) a comparison between D_{tis} obtained by MC calculations with D_{w} calculated with conventional TPS, and their transfer method, or vice versa, is necessary to take into account D_{w}-based previous clinical experience.

TG-43 photon brachytherapy dosimetry assumes that:

(1) The source is located in an infinite water medium and CPE exists (except in the vicinity of the source capsule).
(2) The absorbed dose to a point in tissue located in such a water infinite medium, D_{tis}, is approximated by the collision kerma, $(K_{\mathrm{col}})_{\mathrm{tis}}$, at the same point, i.e.:

$$D_{\mathrm{tis}} \overset{\mathrm{CPE}}{=} (K_{\mathrm{col}})_{\mathrm{tis}} = \Psi_{\mathrm{tis}} \, (\bar{\mu}_{\mathrm{en}}/\rho)_{\mathrm{tis}} \tag{1}$$

where $(\bar{\mu}_{\mathrm{en}}/\rho)_{\mathrm{tis}}$ is the mass energy-absorption coefficient, averaged over the photon energy-fluence spectrum, and $\Psi_{\mathrm{tis}} = \int_E \Psi_E^{\mathrm{tis}} \mathrm{d}E$ is the total photon energy-fluence, with

$$\Psi_E^{\text{tis}} = \left.\frac{\mathrm{d}\Psi}{\mathrm{d}E}\right|_{\text{tis}} = E\,\Phi_E^{\text{tis}} = E\left.\frac{\mathrm{d}\Phi}{\mathrm{d}E}\right|_{\text{tis}} \tag{2}$$

Φ_E^{tis} being the photon fluence spectrum, differential in energy, at the point of interest in tissue.

(3) The relation between dose-to-water, D_{w}, and dose-to-tissue D_{tis} can therefore be written as

$$\frac{D_{\text{w}}}{D_{\text{tis}}} = \frac{\Psi_{\text{w}}}{\Psi_{\text{tis}}}\frac{(\bar{\mu}_{\text{en}}/\rho)_{\text{w}}}{(\bar{\mu}_{\text{en}}/\rho)_{\text{tis}}} \tag{3}$$

where Ψ_{w} and Ψ_{tis} are the total photon energy-fluences in water and in tissue, respectively, and $(\bar{\mu}_{\text{en}}/\rho)_{\text{w}}$ and $(\bar{\mu}_{\text{en}}/\rho)_{\text{tis}}$ are the mass energy-absorption coefficients of water and tissue, averaged over the local photon energy-fluence.

(4) Assuming, as it is widely done, that the photon energy-fluence at the point of interest is practically the same in tissue and in water, i.e. that the ratio $\Psi_{\text{w}}/\Psi_{\text{tis}} \cong 1$, equation (3) becomes:

$$\frac{D_{\text{w}}}{D_{\text{tis}}} = (\bar{\mu}_{\text{en}}/\rho)_{\text{tis}}^{\text{w}} \tag{4}$$

where $(\bar{\mu}_{\text{en}}/\rho)_{\text{tis}}^{\text{w}}$ is the ratio of mass energy-absorption coefficients of water and tissue, averaged over the local photon energy-fluence.

(5) If, on the other hand, the photon energy-fluence depends on the medium at the point of interest, the ratio $\Psi_{\text{w}}/\Psi_{\text{tis}}$ needs to be taken into account, so that equation (3) can be written as:

$$\frac{D_{\text{w}}}{D_{\text{tis}}} = \Psi_{\text{tis}}^{\text{w}}\,(\bar{\mu}_{\text{en}}/\rho)_{\text{tis}}^{\text{w}} \tag{5}$$

where $\Psi_{\text{tis}}^{\text{w}}$ is the ratio of the total photon energy-fluences in water and tissue, which in this work is termed the *water-to-tissue photon energy-fluence correction factor*, and $(\bar{\mu}_{\text{en}}/\rho)_{\text{tis}}^{\text{w}}$ has the same meaning as above.

We will henceforth explore the relations (4) and (5) for various human body tissues in the energy region of interest for certain brachytherapy sources. To do so, we will compute D_{w}, D_{tis}, $\Psi_{\text{tis}}^{\text{w}}$, and $(\bar{\mu}_{\text{en}}/\rho)_{\text{tis}}^{\text{w}}$ as described in what follows.

2.2. Monte Carlo calculations

MC calculations were performed using the PENELOPE MC system version 2014 (Salvat 2014), henceforth referred to as PEN14, which accurately models photon and electron interactions in an arbitrary material for the energy range of interest in this work. This system has already been successfully applied for dosimetric studies in the field of brachytherapy (Granero *et al* 2011). A comparison of PENELOPE MC results with experimental data has been reported elsewhere (Sempau *et al* 2003). PEN14 photon cross-sections for Rayleigh scattering are extracted from the EPDL97 cross sections library (Cullen *et al* 1997, Perkins *et al* 2001). For incoherent (Compton) scattering PENELOPE uses the impulse approximation of Ribberfors (1975), which includes binding effects and Doppler broadening, i.e. for a given scattering angle, the cross section yields a photon energy distribution rather than the single photon energy resulting from the scattering of a photon with a free electron (the classical *Compton line*). Photoelectric cross-sections are calculated with the program *photoabs* (Sabbatucci and Salvat 2016), which uses the same theory as in the re-normalized calculations

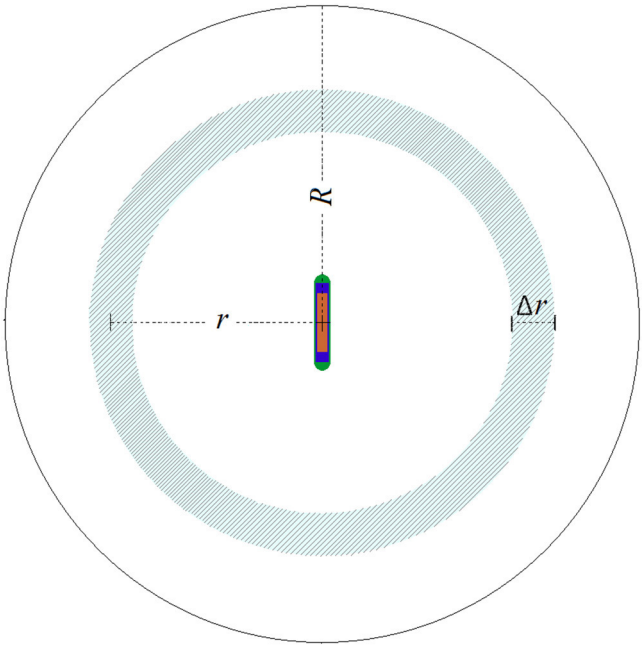

Figure 1. Schematic illustration of the simulation geometry, the size of the phantom is a water sphere with $R = 30$ cm, the thickness of the detectors is $\Delta r = 0.2$ cm, and the source-centre to detector distance r is 1 cm or 5 cm (figure not to scale).

by Scofield (1978), but implementing more accurate numerical algorithms and an extended energy range. A comparison of mass energy-absorption coefficients for different materials using this photon dataset and values from other libraries (e.g. the widely used NIST database, see www.nist.gov/pml/x-ray-mass-attenuation-coefficients) has been described by Andreo *et al* (2012). Electron cross-sections are directly calculated by the PENELOPE data generation code *pendbase* and, for this work, updated mean excitation energies (I-values) and mass density for water and carbon have been used for the evaluation of the density effect in stopping power calculations (Andreo *et al* 2013, ICRU 2016).

2.2.1. Low-energy brachytherapy seeds. Three brachytherapy low-energy seeds have been investigated in this study:

(1) Model IAPd -103A ^{103}Pd source (IsoAid LLC, Port Richey, FL, USA),
(2) Model 6711 ^{125}I source (GE Healthcare, IL. Marketed by Oncura, Inc), and
(3) Model Cs-1 Rev2 ^{131}Cs source (IsoRay Medical, Richland, WA).

The seeds were modelled according to published descriptions (Dolan *et al* 2006, Rivard 2007, Sowards 2007) and the primary radionuclide spectra were obtained from the USA national nuclear data center (NNDC); the mean photon energies for the ^{103}Pd, ^{125}I and ^{131}Cs spectra are 20.8 keV, 28.5 keV and 30.4 keV, respectively (Baglin 2012).

2.2.2. Materials and geometry of the Monte Carlo calculations. Figure 1 shows the geometric modelling used for the study, which consists of an 'infinite' water sphere ($R = 30$ cm) containing a spherical shell detector of thickness $\Delta r = 0.2$ cm (hatched area) with the seed located at its centre. The shell thickness corresponds approximately to the continuous

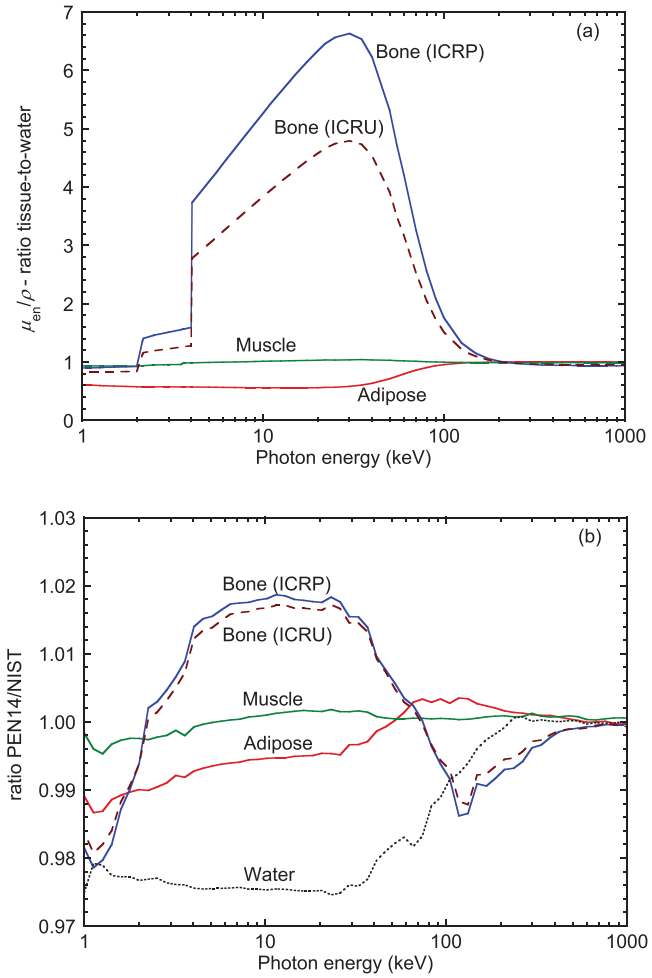

Figure 2. (a) Mass energy-absorption coefficients of various human tissues relative to water calculated in this work using the *mutren* code of the PENELOPE 2014 MC system (Salvat 2014), as a function of the photon energy. (b) Quotients of the PEN14 ratios to the corresponding NIST values (Seltzer, private communication); μ_{en}/ρ-ratios for water in the two databases, where the NIST data correspond to the non-re-normalized values given in ICRU (2016), are included for completeness.

slowing down range in water of the maximum possible electron energy of the ^{103}Pd source ($R_{\mathrm{CSDA,497\,keV}} = 0.18$ cm). In this study, two different 'detector' locations were used. In the first one, the detector was located at a distance $r = 1$ cm of the seed centre (the typical prescription distance), and in the second one at a distance $r = 5$ cm (a typical distance for the organs at risk). These detectors were used to score photon energy-fluence spectra differential in energy and absorbed doses in the MC calculations.

The material of the spherical detectors were water and four human tissues of interest in brachytherapy: muscle, adipose tissue and two types of bone, cortical bone with composition from ICRP (2009) and skeletal bone from ICRU (1992). The reason for including two different bone compositions is due to the significant difference between mass energy-absorption coefficients in relation to water despite having the same mass density (see figure 2). The same

Table 1. Materials composition (in fraction by weight) and relevant atomic properties.

Material	Water	Muscle	Adipose tissue	Cortical bone (ICRP)	Skeletal bone (ICRU)
H	1.12×10^{-1}	1.01×10^{-1}	1.19×10^{-1}	4.72×10^{-2}	6.39×10^{-2}
C	—	1.08×10^{-1}	6.37×10^{-1}	1.44×10^{-1}	2.78×10^{-1}
N	—	2.77×10^{-2}	7.97×10^{-3}	4.19×10^{-2}	2.70×10^{-2}
O	8.80×10^{-1}	7.55×10^{-1}	2.32×10^{-1}	4.46×10^{-1}	4.10×10^{-1}
Mg	—	1.90×10^{-4}	2.00×10^{-5}	2.20×10^{-3}	2.00×10^{-3}
P	—	1.80×10^{-3}	1.60×10^{-4}	1.05×10^{-1}	7.00×10^{-2}
S	—	2.41×10^{-3}	7.30×10^{-4}	3.15×10^{-3}	2.00×10^{-3}
Cl	—	7.90×10^{-4}	1.19×10^{-3}	—	—
K	—	3.02×10^{-3}	3.20×10^{-4}	—	—
Ca	—	3.00×10^{-5}	2.00×10^{-5}	2.09×10^{-1}	1.47×10^{-1}
Others	—	6.00×10^{-5}	5.00×10^{-4}	4.55×10^{-3}	1.00×10^{-4}
ρ Z/A	0.5540	0.5714	0.5138	0.9644	0.9807
Density (g cm^{-3})	0.998	1.04	0.92	1.85	1.85
I-value (eV)	78	75.3	63.2	106.4	91.9

is true for the different electron mass stopping powers and scattering power of the two bone tissues where, due to their different atomic composition, electron density and mean excitation energy, the quantities $(S/\rho)_{\text{bone}}$ and $(T/\rho)_{\text{bone}}$ are quite different. The required tissue/material data files for this work were consistently created using the PENELOPE/ *pendbase* code. The atomic composition, mass density and I-values of each material are given in table 1.

2.2.3. Monte Carlo simulation parameters. The electron-transport algorithm in PENELOPE is governed by five user-defined simulation parameters for each material, namely E_{ABS}, C_1, C_2, W_{CC}, and W_{CR}:

– Parameter E_{ABS} defines when the track evolution stops and the kinetic energy of the particle is deposited locally. (A corresponding parameter is used for photon transport, see below).
– Parameters C_1 and C_2 correspond to the average angular deflection and the maximum average fractional energy loss per step, respectively, and they were set to 0.05 as recommended by the user manual for an optimal compromise between calculation speed and accuracy.
– Parameters W_{CC} and W_{CR} specify the energy cut-offs for hard inelastic and radiative collisions, respectively; both were set to 0.

Photons and electrons were transported down to an energy cut-off $E_{\text{ABS}} = 1$ keV. The number of incident photons was set to 10^9 for all calculations, so that the Type A standard uncertainties of the MC-scored absorbed dose and of the total fluence were 0.5% and 0.01%, respectively, the latter being estimated from the propagation of the uncertainties of each fluence bin.

2.2.4. Estimators of photon energy-fluence spectra and absorbed dose. The PenEasy user code (Sempau *et al* 2011), based on the PENELOPE system, was used to perform the MC calculations. Two tallies were employed:

– The 'tallyFluenceTrackLength' was used to calculate the average photon track-length spectra within the detector volume, whose output is given multiplied by the detector

volume, $V\Phi_E$, V being the detector volume (the score was subsequently divided by V). Photon fluence spectra Φ_E in water and in each tissue were scored for $\Delta E = 0.25$ keV from $E_{\min}$ to $E_{\max}$, the minimum and the maximum energies of each incident seed spectrum. Subsequently, the energy-fluence differential in energy Ψ_E was determined from Φ_E (see equation (2)).

– The 'tallySphericalDoseDistribution' was used to score the absorbed doses $D_{\rm w}$ and $D_{\rm tis}$ inside the two detector volumes.

Additionally, the *mutren* code of PENELOPE was used to calculate $\mu_{\rm en}/\rho$ for water and each tissue for the energy of each bin, E_i.

2.3. Ratios of mass energy-absorption coefficients of water and tissue and photon energy-fluence spectra

Using the equations given in section 2.1 together with the MC-scored quantities obtained as described in section 2.2, the ratio water-to-tissue of the energy-fluence weighted average mass energy-absorption coefficients were evaluated according to:

$$\left(\bar{\mu}_{\rm en}/\rho\right)^{\rm w}_{\rm tis} = \frac{\dfrac{\int_{E_{\min}}^{E_{\max}} \Psi^{\rm w}_E [\mu_{\rm en}(E_i)/\rho]_{\rm w}\,{\rm d}E}{\int_{E_{\min}}^{E_{\max}} \Psi^{\rm w}_E\,{\rm d}E}}{\dfrac{\int_{E_{\min}}^{E_{\max}} \Psi^{\rm tis}_E [\mu_{\rm en}(E_i)/\rho]_{\rm tis}\,{\rm d}E}{\int_{E_{\min}}^{E_{\max}} \Psi^{\rm tis}_E\,{\rm d}E}} \cong \frac{\dfrac{\sum_{i=1}^{n} \Psi^{\rm w}_{E_i} [\mu_{\rm en}(E_i)/\rho]_{\rm w}}{\sum_{i=1}^{n} \Psi^{\rm w}_{E_i}}}{\dfrac{\sum_{i=1}^{n} \Psi^{\rm tis}_{E_i} [\mu_{\rm en}(E_i)/\rho]_{\rm tis}}{\sum_{i=1}^{n} \Psi^{\rm tis}_{E_i}}} \tag{6}$$

where $\Psi^{\rm w}_{E_i}$ and $\Psi^{\rm tis}_{E_i}$ are the energy-fluence distributions in water and tissue, respectively, and n is the number of energy bins required to cover the energy range using $\Delta E = 0.25$ keV.

Following the same procedure, the values of the $\Psi^{\rm w}_{\rm tis}$-ratios were calculated using

$$\Psi^{\rm w}_{\rm tis} = \frac{\int_{E_{\min}}^{E_{\max}} \Psi^{\rm w}_E\,{\rm d}E}{\int_{E_{\min}}^{E_{\max}} \Psi^{\rm tis}_E\,{\rm d}E} \cong \frac{\frac{1}{n}\sum_{i=1}^{n} \Psi^{\rm w}_{E_i}}{\frac{1}{n}\sum_{i=1}^{n} \Psi^{\rm tis}_{E_i}} \tag{7}$$

Taking into account the uncertainty of the MC-calculated total fluences in water and in tissue, a conservative estimate for the Type A standard uncertainty of the water-to-tissue photon energy-fluence correction factor is 0.02%.

3. Results and discussion

The PEN14-calculated mass energy-absorption coefficients of the human tissues relative to those of water are shown in figure 2(a) as a function of the photon energy. For comparison, the quotient between the data from PEN14 and the corresponding NIST-values (Seltzer, private communication; note that the ICRP tissue compositions used in this work are not included in the web-based NIST database) is presented in figure 2(b), which shows discrepancies of up to ±2% mostly for the two bone tissues. It should be noted that the differences shown in the latter figure are not solely due to the photoeffect cross sections in each dataset, re-normalized in PEN14 and non-re-normalized in NIST, but also to the use of the impulse approximation for Compton scattering and its account for Doppler broadening in PENELOPE whereas the NIST data uses the Klein–Nishina kinematics relationship for the scattered photon (Compton

line). Both datasets incorporate binding effects. For completeness, figure 2(b) also includes the ratios PEN14/NIST for water, where the NIST data correspond to the non-re-normalized XCOM values given in ICRU (2016).

The PEN14 calculated values have been used in combination with the photon energy-fluence spectra calculated in the 'detectors' at a distance of 1 cm and 5 cm from the seed centre. The energy-fluence weighted average mass energy-absorption coefficients ratios were calculated according to equation (6) using the following energy limits for each source:

(1) ^{103}Pd: $E_{\min} = 0.5$ keV and $E_{\max} = 497.08$ keV
(2) ^{125}I: $E_{\min} = 0.5$ keV and $E_{\max} = 35.492$ keV
(3) ^{131}Cs: $E_{\min} = 0.5$ keV and $E_{\max} = 34.419$keV

and the results are summarized in table 2.

For the PEN14 calculated photon spectra, differences in the energy-fluence weighted average $(\bar{\mu}_{\text{en}}/\rho)^{\text{w}}_{\text{tis}}$, see equation (6), using PEN14 and NIST μ_{en}/ρ data, vary within -2.1% (^{125}I, bone ICRP) and 0.7% (^{125}I, adipose tissue), with an overall mean difference of -0.9%. It should be noted, however, that the resulting Type B uncertainty due to this mean difference ($u_{\text{B,95\% c.l.}} \approx 0.7\%$, see Andreo *et al* (2012)) is applicable to the values in table 2, but does not play a significant role in the energy-fluence correction factors obtained from equation (7), as these depend on the MC-calculated photon spectra, which are expected to be approximately similar using both datasets, but not on μ_{en}/ρ values. Resolving this approximation would require two MC spectra calculations (for each case) with the same MC code but using different photon cross sections, a task beyond the scope of the present work.

Energy-fluence ratios $\Psi^{\text{w}}_{\text{tis}}$ obtained using equation (7) are given in table 3, where it can be seen that only the muscle/water ratios are approximately close to one. For the different sources and the two distances, in adipose tissue the energy-fluence ratio to water varies within about -3% and -1%, but it varies up to within 20% and 50% (ICRU), and to within 26% and 72% (ICRP), for the two bone compositions. Such large differences show that the common assumption of considering approximately equal the fluences in water (or in a soft tissue like muscle) and in bone, that provides the basis for a dose ratio equal to that of the mass energy-absorption coefficients (see equation 4), is a poor approximation for high-Z tissues. Note that the results for the two different compositions of bone, both with the same density, question the adequacy of density versus tissue lookup tables for tissue characterization (see Andreo (2015)).

The proposal in this work is therefore to include a photon energy-fluence correction factor $\Psi^{\text{w}}_{\text{tis}}$ to account for the fluence difference in two media according to equation (5). This correction parallels the proposal made by Andreo (2015) for megavoltage photon beams, where an electron fluence correction was introduced for the tissues used in the present work. The correction factors are however, substantially larger in the case of low-energy photons used in brachytherapy than in megavoltage photons.

Recall that our goal is to determine a 'converted' absorbed dose to water, $D^{\text{conv}}_{\text{w}}$, using an advanced TPS-calculated $D^{\text{TPS}}_{\text{tis}}$, e.g. by MC simulation, that is, one deals with a process $D^{\text{MC}}_{\text{tis}} \rightarrow D^{\text{conv}}_{\text{w}}$. The two approximations given in equations (4) and (5) can, respectively, be written for this process as

$$D^{\text{conv}}_{\text{w}} = D^{\text{MC}}_{\text{tis}} \, (\bar{\mu}_{\text{en}}/\rho)^{\text{w}}_{\text{tis}} \tag{8}$$

and

$$D^{\text{conv}}_{\text{w}} = D^{\text{MC}}_{\text{tis}} \, (\bar{\mu}_{\text{en}}/\rho)^{\text{w}}_{\text{tis}} \, \Psi^{\text{w}}_{\text{tis}} \tag{9}$$

Table 2. Energy-fluence weighted average mass energy-absorption coefficients of different tissues, and their ratio relative to that of water, evaluated for the ^{125}I, ^{131}Cs and ^{103}Pd spectra. The estimated standard uncertainty of the $(\bar{\mu}_{en}/\rho)^{w}_{tis}$ values is 0.7%.

	1 cm						5 cm					
	^{125}I		^{131}Cs		^{103}Pd		^{125}I		^{131}Cs		^{103}Pd	
Materials	$(\bar{\mu}_{en}/\rho)$ (cm^2 g^{-1})	$(\bar{\mu}_{en}/\rho)^{w}_{tis}$	$(\bar{\mu}_{en}/\rho)$ (cm^2 g^{-1})	$(\bar{\mu}_{en}/\rho)^{w}_{tis}$	$(\bar{\mu}_{en}/\rho)$ (cm^2 g^{-1})	$(\bar{\mu}_{en}/\rho)^{w}_{tis}$	$(\bar{\mu}_{en}/\rho)$ (cm^2 g^{-1})	$(\bar{\mu}_{en}/\rho)^{w}_{tis}$	$(\bar{\mu}_{en}/\rho)$ (cm^2 g^{-1})	$(\bar{\mu}_{en}/\rho)^{w}_{tis}$	$(\bar{\mu}_{en}/\rho)$ (cm^2 g^{-1})	$(\bar{\mu}_{en}/\rho)^{w}_{tis}$
Water	0.218	1.000	0.158	1.000	0.492	1.000	0.212	1.000	0.173	1.000	0.387	1.000
Muscle	0.227	0.961	0.165	0.960	0.509	0.967	0.220	0.961	0.180	0.961	0.400	0.968
Adipose	0.125	1.734	0.092	1.711	0.278	1.770	0.122	1.729	0.100	1.715	0.221	1.754
Bone (skeletal, ICRU)	1.016	0.214	0.754	0.210	2.237	0.220	0.982	0.216	0.807	0.214	1.595	0.242
Bone (cortical, ICRP)	1.391	0.156	1.035	0.153	3.066	0.160	1.344	0.157	1.105	0.156	2.101	0.184

Table 3. Energy-fluence weighted average photon total energy-fluence and energy-fluence correction factors for different tissues, evaluated for the ^{125}I, ^{131}Cs and ^{103}Pd spectra. The estimated Type A standard uncertainty of the Ψ_{tis}^{w} values is 0.02%.

	1 cm						5 cm					
	^{125}I		^{131}Cs		^{103}Pd		^{125}I		^{131}Cs		^{103}Pd	
	Ψ (eV cm^{-2})	Ψ_{tis}^{w}	Ψ (eV cm^{-2})	Ψ_{tis}^{w}	Ψ (eV cm^{-2})	Ψ_{tis}^{w}	Ψ (eV cm^{-2})	Ψ_{tis}^{w}	Ψ (eV cm^{-2})	Ψ_{tis}^{w}	Ψ (eV cm^{-2})	Ψ_{tis}^{w}
Water	917.2	1.000	1263	1.000	459.6	1.000	14.19	1.000	24.91	1.000	2.240	1.000
Muscle	915.6	1.002	1261	1.001	457.8	1.004	14.14	1.003	24.84	1.003	2.230	1.003
Adipose	930.0	0.986	1275	0.990	474.2	0.969	14.48	0.979	25.36	0.982	2.310	0.970
Bone (skeletal, ICRU)	742.1	1.236	1070	1.180	307.8	1.493	10.89	1.302	19.68	1.266	1.600	1.397
Bone (cortical, ICRP)	683.0	1.343	999.8	1.263	266.6	1.724	9.940	1.427	18.11	1.376	1.440	1.555

Table 4. Data for MC-calculated ratio $\frac{D_{\text{tis}}^{\text{MC}}}{D_{\text{w}}^{\text{MC}}}$ and the approximations of equation (10), $\frac{D_{\text{tis}}^{\text{MC}}}{D_{\text{w}}^{\text{MC}}}(\bar{\mu}_{\text{en}}/\rho)_{\text{tis}}^{\text{w}}$, and equation (11), $\frac{D_{\text{tis}}^{\text{MC}}}{D_{\text{w}}^{\text{MC}}}(\bar{\mu}_{\text{en}}/\rho)_{\text{tis}}^{\text{w}}\,\Psi_{\text{tis}}^{\text{w}}$, for the spectra of ^{125}I, ^{131}Cs and ^{103}Pd seeds at 1 cm.

	1 cm								
	^{125}I			^{131}Cs			^{103}Pd		
Materials	$\frac{D_{\text{tis}}^{\text{MC}}}{D_{\text{w}}^{\text{MC}}}$	$\frac{D_{\text{tis}}^{\text{MC}}}{D_{\text{w}}^{\text{MC}}}(\bar{\mu}_{\text{en}}/\rho)_{\text{tis}}^{\text{w}}$	$\frac{D_{\text{tis}}^{\text{MC}}}{D_{\text{w}}^{\text{MC}}}(\bar{\mu}_{\text{en}}/\rho)_{\text{tis}}^{\text{w}}\,\Psi_{\text{tis}}^{\text{w}}$	$\frac{D_{\text{tis}}^{\text{MC}}}{D_{\text{w}}^{\text{MC}}}$	$\frac{D_{\text{tis}}^{\text{MC}}}{D_{\text{w}}^{\text{MC}}}(\bar{\mu}_{\text{en}}/\rho)_{\text{tis}}^{\text{w}}$	$\frac{D_{\text{tis}}^{\text{MC}}}{D_{\text{w}}^{\text{MC}}}(\bar{\mu}_{\text{en}}/\rho)_{\text{tis}}^{\text{w}}\,\Psi_{\text{tis}}^{\text{w}}$	$\frac{D_{\text{tis}}^{\text{MC}}}{D_{\text{w}}^{\text{MC}}}$	$\frac{D_{\text{tis}}^{\text{MC}}}{D_{\text{w}}^{\text{MC}}}(\bar{\mu}_{\text{en}}/\rho)_{\text{tis}}^{\text{w}}$	$\frac{D_{\text{tis}}^{\text{MC}}}{D_{\text{w}}^{\text{MC}}}(\bar{\mu}_{\text{en}}/\rho)_{\text{tis}}^{\text{w}}\,\Psi_{\text{tis}}^{\text{w}}$
Muscle	1.038	0.997	0.999	1.041	0.999	1.000	1.031	0.997	1.000
Adipose	0.585	1.015	1.001	0.592	1.012	1.002	0.584	1.034	1.003
Bone (skeletal, ICRU)	3.761	0.806	0.996	4.023	0.845	0.998	3.035	0.667	0.997
Bone (cortical, ICRP)	4.739	0.742	0.996	5.164	0.789	0.998	3.600	0.578	0.996

Table 5. Data for MC-calculated ratio $\frac{D_{\text{tis}}^{\text{MC}}}{D_{\text{w}}^{\text{MC}}}$ and the approximations of equation (10), $\frac{D_{\text{tis}}^{\text{MC}}}{D_{\text{w}}^{\text{MC}}}(\bar{\mu}_{\text{en}}/\rho)_{\text{tis}}^{\text{w}}$, and equation (11), $\frac{D_{\text{tis}}^{\text{MC}}}{D_{\text{w}}^{\text{MC}}}(\bar{\mu}_{\text{en}}/\rho)_{\text{tis}}^{\text{w}}\,\Psi_{\text{tis}}^{\text{w}}$, for the spectra of ^{125}I, ^{131}Cs and ^{103}Pd seeds at 5 cm.

	5 cm								
	^{125}I			^{131}Cs			^{103}Pd		
Materials	$\frac{D_{\text{tis}}^{\text{MC}}}{D_{\text{w}}^{\text{MC}}}$	$\frac{D_{\text{tis}}^{\text{MC}}}{D_{\text{w}}^{\text{MC}}}(\bar{\mu}_{\text{en}}/\rho)_{\text{tis}}^{\text{w}}$	$\frac{D_{\text{tis}}^{\text{MC}}}{D_{\text{w}}^{\text{MC}}}(\bar{\mu}_{\text{en}}/\rho)_{\text{tis}}^{\text{w}}\,\Psi_{\text{tis}}^{\text{w}}$	$\frac{D_{\text{tis}}^{\text{MC}}}{D_{\text{w}}^{\text{MC}}}$	$\frac{D_{\text{tis}}^{\text{MC}}}{D_{\text{w}}^{\text{MC}}}(\bar{\mu}_{\text{en}}/\rho)_{\text{tis}}^{\text{w}}$	$\frac{D_{\text{tis}}^{\text{MC}}}{D_{\text{w}}^{\text{MC}}}(\bar{\mu}_{\text{en}}/\rho)_{\text{tis}}^{\text{w}}\,\Psi_{\text{tis}}^{\text{w}}$	$\frac{D_{\text{tis}}^{\text{MC}}}{D_{\text{w}}^{\text{MC}}}$	$\frac{D_{\text{tis}}^{\text{MC}}}{D_{\text{w}}^{\text{MC}}}(\bar{\mu}_{\text{en}}/\rho)_{\text{tis}}^{\text{w}}$	$\frac{D_{\text{tis}}^{\text{MC}}}{D_{\text{w}}^{\text{MC}}}(\bar{\mu}_{\text{en}}/\rho)_{\text{tis}}^{\text{w}}\,\Psi_{\text{tis}}^{\text{w}}$
Muscle	1.037	0.997	0.999	1.038	0.998	1.000	1.029	0.996	1.000
Adipose	0.591	1.022	1.001	0.594	1.019	1.001	0.594	1.042	1.011
Bone (skeletal, ICRU)	3.548	0.766	0.997	3.678	0.787	0.997	2.916	0.707	0.988
Bone (cortical, ICRP)	4.426	0.698	0.996	4.637	0.725	0.997	3.445	0.635	0.987

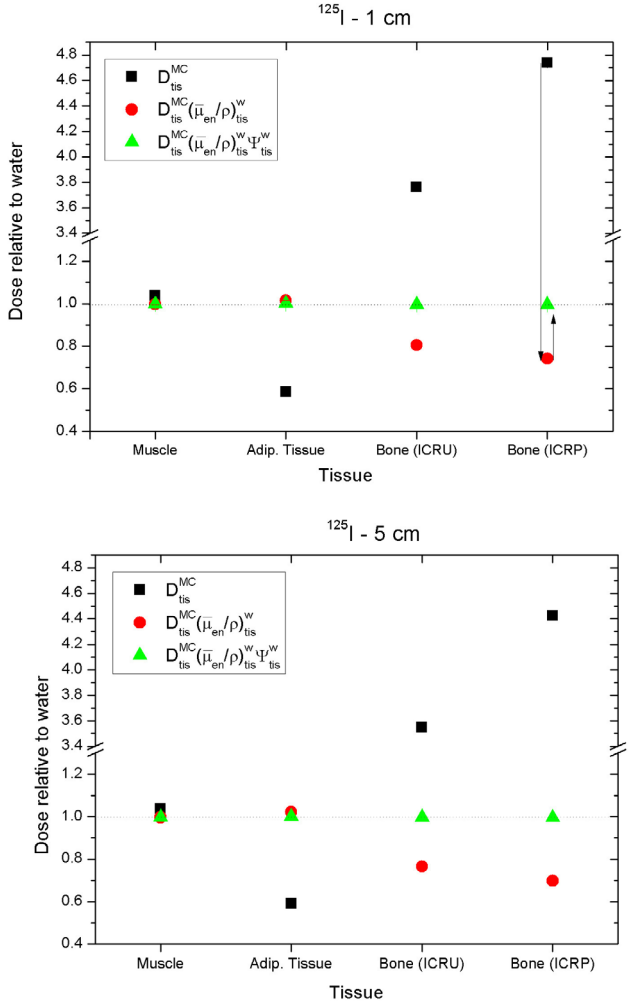

Figure 3. Ratio between $D_{\mathrm{tis}}^{\mathrm{MC}}$ and $D_{\mathrm{w}}^{\mathrm{MC}}$ and the corrections given in equations (10) and (11) for the ^{125}I source. The ratios of the Monte Carlo-scored $D_{\mathrm{tis}}^{\mathrm{MC}}$ and $D_{\mathrm{w}}^{\mathrm{MC}}$ are shown as black squares. Correcting their quotient with the ratio of mass energy-absorption coefficients water-to-tissue yields the red circles. The additional correction with the energy-fluence corrections proposed in this work yields the results shown as green triangles. Type A uncertainties for all the absorbed dose ratios are of the order of 0.5%. The arrows in the upper panel for bone (ICRP) illustrate the trend of dose relative to water when the two different corrections are applied.

where the meaning of the different quantities has been described before.

To verify the validity of each approximation we have also scored $D_{\mathrm{w}}^{\mathrm{MC}}$ in our MC calculations, so that the converted $D_{\mathrm{w}}^{\mathrm{conv}}$ can be compared with this 'reference' $D_{\mathrm{w}}^{\mathrm{MC}}$. An ideal conversion should yield a ratio $D_{\mathrm{w}}^{\mathrm{conv}}/D_{\mathrm{w}}^{\mathrm{MC}} \approx 1$. This ratio can be expressed for both approximations as

$$\frac{D_{\mathrm{w}}^{\mathrm{conv}}}{D_{\mathrm{w}}^{\mathrm{MC}}} = \frac{D_{\mathrm{tis}}^{\mathrm{MC}}}{D_{\mathrm{w}}^{\mathrm{MC}}} (\bar{\mu}_{\mathrm{en}}/\rho)_{\mathrm{tis}}^{\mathrm{w}} \tag{10}$$

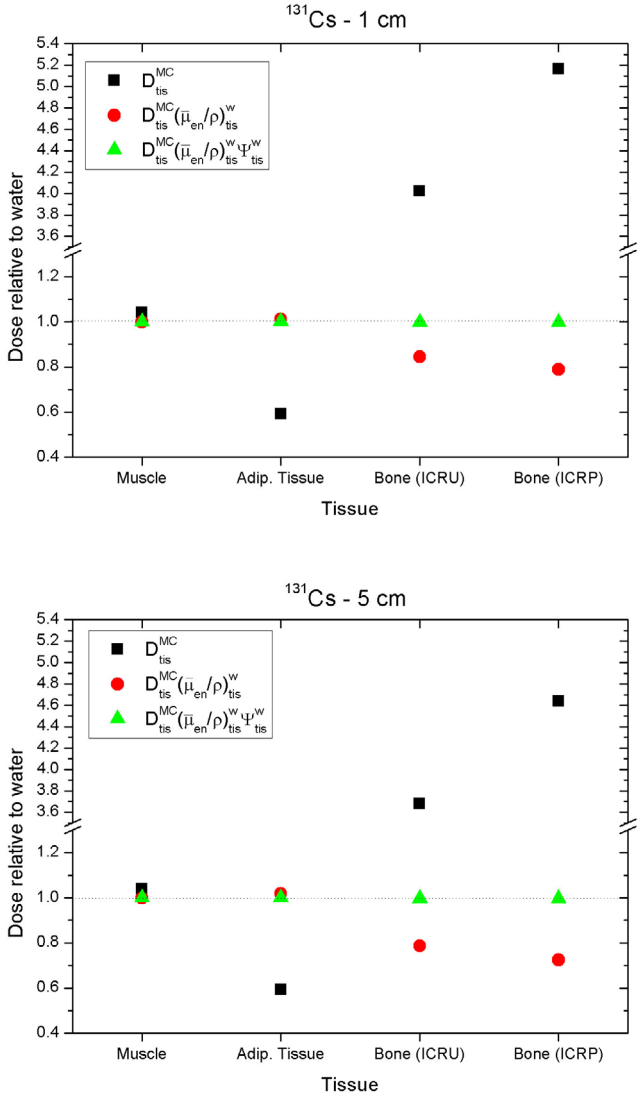

Figure 4. Ratio between D^{MC}_{tis} and D^{MC}_{w} and the corrections given in equations (10) and (11) for the ^{131}Cs source. The ratios of the Monte Carlo-scored D^{MC}_{tis} and D^{MC}_{w} are shown as black squares. Correcting their quotient with the ratio of mass energy-absorption coefficients water-to-tissue yields the red circles. The additional correction with the energy-fluence corrections proposed in this work yields the results shown as green triangles. Type A uncertainties for all the absorbed dose ratios are of the order of 0.5%.

and

$$\frac{D^{conv}_{w}}{D^{MC}_{w}} = \frac{D^{MC}_{tis}}{D^{MC}_{w}} (\bar{\mu}_{en}/\rho)^{w}_{tis} \Psi^{w}_{tis} \tag{11}$$

where all the quantities in the right hand side of both expressions have been derived using our Monte Carlo simulations.

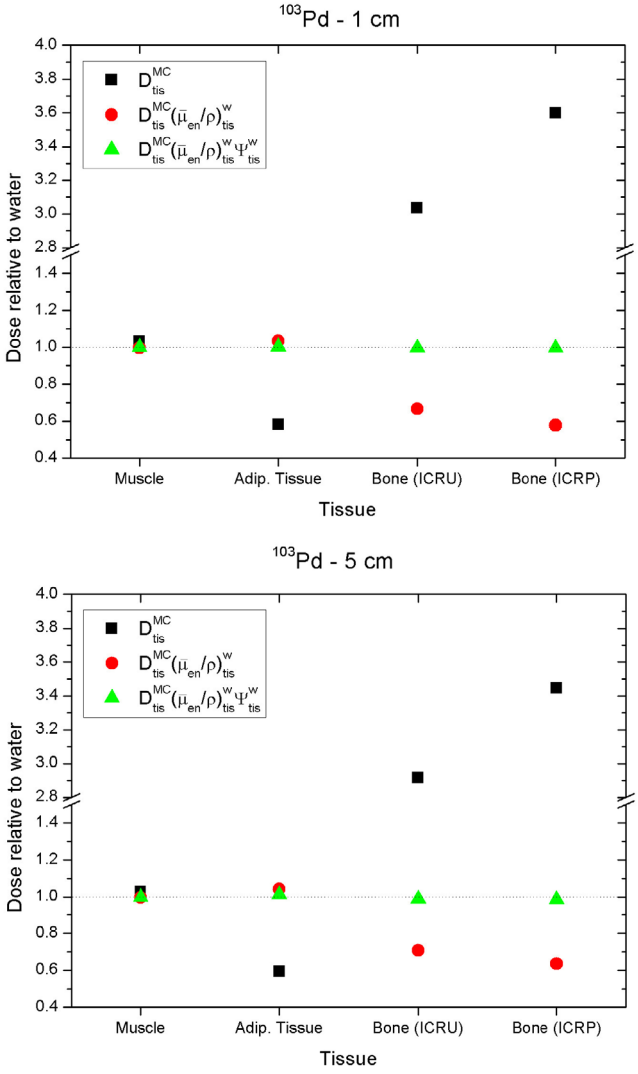

Figure 5. Ratio between D^{MC}_{tis} and D^{MC}_{w} and the corrections given in equations (10) and (11) for the ^{103}Pd source. The ratios of the Monte Carlo-scored D^{MC}_{tis} and D^{MC}_{w} are shown as black squares. Correcting their quotient with the ratio of mass energy-absorption coefficients water-to-tissue yields the red circles. The additional correction with the energy-fluence corrections proposed in this work yields the results shown as green triangles. Type A uncertainties for all the absorbed dose ratios are of the order of 0.5%.

It is emphasized that the flow of steps described above is also valid for the inverse process based on a conventional TPS, i.e. $D^{TPS}_{w} \rightarrow D^{conv}_{tis}$, by making a proper change of the indices involved.

Results for the approximations relating the ratio D^{MC}_{tis}/D^{MC}_{w} of the MC-calculated doses with the corresponding equations (10) and (11), for the spectra from the ^{125}I, ^{131}Cs, and ^{103}Pd sources, and at the distances of 1 cm and 5 cm, are given in tables 4 and 5, respectively. It can be seen that the correction of equation (11) provides dose ratios D^{conv}_{w}/D^{MC}_{w} close to one within

a few tenths of a per cent. The results are also displayed in figures 3–5 for easier visualization, where the top panel of figure 3 illustrates the transition (see the arrows for bone (ICRP), considered to be the most critical case) from the MC-calculated $D_{\mathrm{tis}}^{\mathrm{MC}}/D_{\mathrm{w}}^{\mathrm{MC}}$ to $D_{\mathrm{tis}}^{\mathrm{MC}}\,(\bar{\mu}_{\mathrm{en}}/\rho)_{\mathrm{tis}}^{\mathrm{w}}/D_{\mathrm{w}}^{\mathrm{MC}}$ and to $D_{\mathrm{tis}}^{\mathrm{MC}}\,(\bar{\mu}_{\mathrm{en}}/\rho)_{\mathrm{tis}}^{\mathrm{w}}\,\Psi_{\mathrm{tis}}^{\mathrm{w}}/D_{\mathrm{w}}^{\mathrm{MC}}$.

As an additional verification, the absorbed dose to water and tissues determined using the integral form of equation (1)

$$D_{\mathrm{med}} \cong \int_{E_{\mathrm{min}}}^{E_{\mathrm{max}}} \Psi_E^{\mathrm{med}}\,[\mu_{\mathrm{en}}(E)/\rho]_{\mathrm{med}}\,\mathrm{d}E \tag{12}$$

has been evaluated for the MC-calculated energy-fluence spectra Ψ_E^{med} for each source and the $[\mu_{\mathrm{en}}(E)/\rho]_{\mathrm{med}}$ values used throughout this work. The ratios of this 'large-cavity theory' D_{med} to the directly MC-calculated $D_{\mathrm{med}}^{\mathrm{MC}}$ agree on the average within 0.2%, the range being (−2.5%, +0.7%) with the largest difference corresponding to ^{103}Pd and adipose tissue at 5 cm. The corresponding Type B standard uncertainty estimate of the D_{med} values is 0.8%, this being also a conservative estimate of the dose ratios $D_{\mathrm{med}}^{\mathrm{MC}}/D_{\mathrm{w}}^{\mathrm{MC}}$ in tables 4 and 5 due to the correlation of the two quantities (same method and MC code).

The different dose ratios have been analysed at 1 cm and 5 cm from the source centre in order to distinguish whether the proposed corrections could be used for clinically relevant distances, less than 5 cm from the source. The results obtained show that the calculated energy-fluence correction factors can be used to establish a relationship between absorbed dose to tissue and absorbed dose to water for a broad range of clinically relevant distances.

As expected, any advanced TPS based e.g. on a MC simulation, will yield significant differences between $D_{\mathrm{tis}}^{\mathrm{MC}}$ and $D_{\mathrm{w}}^{\mathrm{MC}}$ for all sources and tissues, especially for bone. $D_{\mathrm{tis}}^{\mathrm{MC}}$ values can be approximately 3.5 times higher than $D_{\mathrm{w}}^{\mathrm{MC}}$ for the two types of bone tissue (ICRP and ICRU compositions). The energy-fluence based correction proposed in equation (11) provides an excellent estimation of the correction needed to the ratio $D_{\mathrm{tis}}^{\mathrm{MC}}/D_{\mathrm{w}}^{\mathrm{MC}}$ for the ^{125}I, ^{131}Cs and ^{103}Pd sources used in this work and for all clinically relevant distances with an standard uncertainty estimate better than 0.1%. Taking into account this estimate and that of the dose ratios (∼0.8%) and of the $(\bar{\mu}_{\mathrm{en}}/\rho)_{\mathrm{tis}}^{\mathrm{w}}$ values (∼0.7%), the combined standard uncertainty for the entire set of calculations in this work is about 1%, of which only one tenth corresponds to the proposed water-to-tissue photon energy-fluence correction factor.

4. Conclusions

A photon energy-fluence based correction has been proposed that represents an straightforward and efficient procedure to correlate absorbed dose to water and absorbed dose to tissue in brachytherapy calculations for clinically relevant distances and radionuclides. Its rationale is that photon fluence varies in different media, particularly between water and high-Z tissues like bone; for adipose tissues the differences are much smaller but still worth correcting for. The corrections provided can be implemented in any treatment planning system and be easily extended to other distances, sources and/or radionuclides by performing a detailed MC simulation following the procedures outlined in this work. For the new MBDCA calculation techniques, photon fluence estimators can be included in the calculation process so that both absorbed dose and photon fluence are scored simultaneously; outputs can then be given in terms of dose to tissue and of dose to water in an accurate way.

Acknowledgments

This work was supported in part by Generalitat Valenciana under Project PROMETEOII/2013/010, by the Spanish Government under Project No. FIS2013-42156. PCGA is grateful to acknowledge CNPq-Brazil for a research fellowship. S. Seltzer is gratefully acknowledged for providing μ_{en}/ρ data for the different tissues calculated according to the NIST database.

References

Afsharpour H *et al* 2011 Tissue modelling schemes in low energy breast brachytherapy *Phys. Med. Biol.* **56** 7045–60

Ahnesjö A 2013 Collapsed cone convolution of radiant energy for photon dose calculation in heterogeneous media *Med. Phys.* **16** 577–92

Andreo P 2015 Dose to 'water-like' media or dose to tissue in MV photons radiotherapy treatment planning: still a matter of debate *Phys. Med. Biol.* **60** 309–337

Andreo P 2015 Dose to 'water-like' media or dose to tissue in MV photons radiotherapy treatment planning: still a matter of debate *Phys. Med. Biol.* **60** 2619 (corrigendum)

Andreo P, Burns D T and Salvat F 2012 On the uncertainties of photon mass energy-absorption coefficients and their ratios for radiation dosimetry *Phys. Med. Biol.* **57** 2117–36

Andreo P, Wulff J, Burns D T and Palmans H 2013 Consistency in reference radiotherapy dosimetry: resolution of an apparent conundrum when ^{60}Co is the reference quality for charged-particle and photon beams *Phys. Med. Biol.* **58** 6593–621

Attix F H 1986 *Introduction to Radiological Physics and Radiation Dosimetry* (New York: Wiley)

Baglin C M 2012 Nuclear data sheets for $A = 192$ *Nucl. Data Sheets* **113** 1871–2111

Ballester F *et al* 2015 A generic high-dose rate ^{192}Ir brachytherapy source for evaluation of model-based dose calculations beyond the TG-43 formalism *Med. Phys.* **42** 3048–62

Beaulieu L *et al* 2012 Report of the task group 186 on model-based dose calculation methods in brachytherapy beyond the TG-43 formalism: current status and recommendations for clinical implementation *Med. Phys.* **39** 6208–36

Carlsson-Tedgren A and Alm-Carlsson G 2013 Specification of absorbed dose to water using model-based dose calculation algorithms for treatment planning in brachytherapy *Phys. Med. Biol* **58** 2561–79

Carlsson-Tedgren A and Ahnesjö A 2008 Optimization of the computational efficiency of a 3D, collapsed cone dose calculation algorithm for brachytherapy *Med. Phys.* **35** 1611

Cullen D E, Hubbell J H and Kissel L 1997 *EPDL97: the Evaluated Photon Data Library* (Livermore, CA: Lawrence Livermore National Laboratory)

Dolan J, Li Z and Williamson J F 2006 Monte Carlo and experimental dosimetry of an ^{125}I brachytherapy seed *Med. Phys.* **33** 4675–4684

Fonseca G P *et al* 2015 Dose specification for ^{192}Ir high dose rate brachytherapy in terms of dose-to-water-in-medium and dose-to-medium-in-medium *Phys. Med. Biol.* **60** 4565–79

Granero D *et al* 2011 Dosimetry revisited for the HDR ^{192}Ir brachytherapy source model mHDR-v2 *Med. Phys.* **38** 487–94

ICRP 2009 Adult reference computational phantoms ICRP Publication 110 *Ann. ICRP* **39** 2

ICRU 1992 *Photon, Electron, Proton and Neutron Interaction Data for Body Tissues* (*ICRU Report* vol 46) (Bethesda, MD: International Commission on Radiation Units and Measurements)

ICRU 2016 *Key Data for Ionizing Radiation Dosimetry: Measurement Standards and Applications* (*ICRU Report* vol 90) (Bethesda, MD: International Commission on Radiation Units and Measurements)

Kumar S, Deshpande D D and Nahum A E 2016 Dosimetric response of variable-size cavities in photon-irradiated media and the behaviour of the Spencer–Attix cavity integral with increasing Δ *Phys. Med. Biol.* **61** 2680–704

Landry G *et al* 2011 The difference of scoring dose to water or tissues in Monte Carlo dose calculations for low energy brachytherapy photon sources *Med. Phys.* **38** 1526–33

Lloyd S A M and Ansbacher W 2013 Evaluation of an analytic linear Boltzmann transport equation solver for high-density inhomogeneities *Med. Phys.* **40** 11707

Nath R *et al* 1995 Dosimetry of interstitial brachytherapy sources: recommendations of the AAPM radiation therapy committee task group no 43 *Med. Phys.* **22** 209–34

Perez-Calatayud J *et al* 2012 Dose calculation for photon-emitting brachytherapy sources with average energy higher than 50 keV: report of the AAPM and ESTRO *Med. Phys.* **39** 2904–29

Perkins S T, Cullen D E and Seltzer S M 2001 *Tables and Graphs of Electron-Interaction Cross-Sections from 10 eV to 100 GeV Derived from the LLNL Evaluated Electron Data Libray Z = 1–100* (Livermore, CA: Lawrence Livermore National Laboratory)

Petrokokkinos L *et al* 2011 Dosimetric accuracy of a deterministic radiation transport based ^{192}Ir brachytherapy treatment planning system. Part II: Monte Carlo and experimental verification of a multiple source dwell position plan employing a shielded applicator *Med. Phys.* **38** 1981–92

Ribberfors R 1975 Relationship of the relativistic Compton cross section to the momentum distribution of bound electron states *Phys. Rev.* B **12** 2067–74

Rivard M J 2007 Brachytherapy dosimetry parameters calculated for a ^{131}Cs source *Med. Phys.* **34** 754–62

Rivard M J *et al* 2006 Calculated and measured brachytherapy dosimetry parameters in water for the Xoft Axxent x-ray source: an electronic brachytherapy source *Med. Phys.* **33** 4020–32

Rivard M J *et al* 2004 Update of AAPM task group no. 43 report: a revised AAPM protocol for brachytherapy dose calculations *Med. Phys.* **31** 633–74

Rivard M J, Beaulieu L and Mourtada F 2010 Enhancements to commissioning techniques and quality assurance of brachytherapy treatment planning systems that use model-based dose calculation algorithms *Med. Phys.* **37** 2645–58

Sabbatucci L and Salvat F 2016 Theory and calculation of the atomic photoeffect *Radiat. Phys. Chem.* **121** 122–140

Salvat F 2014 *PENELOPE. A Code System for Monte Carlo Simulation of Electron and Photon Transport* (Issy-Les-Moulineaux: OECD Nuclear Energy Agengy)

Scofield J H 1978 K-and L-shell ionization of atoms by relativistic electrons *Phys. Rev.* A **18** 963–70

Sempau J *et al* 2003 Experimental benchmarks of the Monte Carlo code PENELOPE *Nucl. Instrum. Methods* B **207** 107–123

Sempau J, Badal A and Brualla L 2011 A PENELOPE based system for the automated Monte Carlo simulation of clinacs and voxelized geometries, application to far from axis fields *Med. Phys.* **38** 5887

Sowards K T 2007 Monte Carlo dosimetric characterization of the IsoAid ADVANTAGE ^{103}Pd brachytherapy source *J. Appl. Clin. Med. Phys.* **8** 18–25

Sutherland J G H *et al* 2012 Model-based dose calculations for ^{125}I lung brachytherapy *Med. Phys.* **39** 4365

Van Veelen B, Ma Y and Beaulieu L 2014 ACE advanced collapsed cone engine ELEKTA White paper available at www.elekta.com